ELSEVIER

International Journal of Solids and Structures 41 (2004) 5411–5424

INTERNATIONAL JOURNAL OF SOLIDS and STRUCTURES

www.elsevier.com/locate/ijsolstr

A new constitutive model for the phase transformations in mono-crystalline silicon

T. Vodenitcharova *, L.C. Zhang *

School of Aerospace, Mechanical and Mechatronic Engineering, The University of Sydney, Sydney NSW 2006, Australia

Received 1 March 2003; received in revised form 5 April 2004
Available online 18 May 2004

Abstract

This paper presents a constitutive modelling technique for the multi-phase transformations in mono-crystalline silicon under complex loading. The development is based on the physical mechanisms observed experimentally and the incremental theory of plasticity. The stress–strain relationship is derived using closed loading/unloading surfaces, associated flow rule and isotropic hardening rule, to reflect the pressure-sensitive behaviour of the material with volumetric plastic strains. With the aid of the finite element method, the model is successfully applied to predict the elastic–plastic response of silicon subjected to hydrostatic pressure and nano-indentation, including the phenomena of pop-in and pop-out.

Keywords: Constitutive modelling; Phase transformation; Silicon; Pressure-sensitive materials; Nano-indentation

1. Introduction

Mono-crystalline silicon has been extensively studied in recent years and as many as 12 stable or metastable solid structures of elemental silicon have been experimentally observed at different stress levels or strain rates.

With increasing the hydrostatic pressure in a diamond anvil cell, silicon undergoes various phase transformations whose stress thresholds are dependent on the loading/unloading conditions. In loading at a pressure of 10–12 GPa (Hu et al., 1986) the original diamond structure of silicon (Si I) transforms into a denser β-tin (metallic) phase (Si II), accompanied by a 22% volumetric reduction. A further volumetric decrease of 0.2–0.5% associated with the *Imma* silicon (Si XI) occurs when the pressure reaches the range of 13–16 GPa (McMahon and Nelmes, 1993; McMahon et al., 1994). More phase changes take place upon further increment of the pressure: the primitive hexagonal (ph, Si V) at 14–16 GPa (Hu et al., 1986), *Cmca* (Si VI) at above 38 GPa (Hanfland et al., 1999) and the hexagonal close-packed structure (hcp, Si VII) at

* Corresponding authors. Tel.: +61-2-9351-7145 (T. Vodenitcharova), Tel.: +61-2-9351-2835 (L.C. Zhang); fax: +61-2-9351-7060.
E-mail addresses: tania.v@aeromech.usyd.edu.au (T. Vodenitcharova), zhang@aeromech.usyd.edu.au (L.C. Zhang).

0020-7683/$ - see front matter © 2004 Elsevier Ltd. All rights reserved.
doi:10.1016/j.ijsolstr.2004.04.025

40–49 GPa (Hu et al., 1986). The sequence of the high-pressure phase transformations concludes with the face centered cubic silicon (fcc, Si X) at around 79 GPa (Duclos et al., 1990) which was claimed to remain stable up to 248 GPa.

The above thresholds during loading were determined under pure hydrostatic stress states. When deviatoric stresses were added, the hydrostatic thresholds were lowered (Hu et al., 1986; Wu et al., 1999). This was also confirmed by micro/nano-indentations in which both hydrostatic and deviatoric stresses appear.

Upon hydrostatic unloading, the phase metamorphism of silicon shows a different process. First, the hexagonal close-packed Si changes to ph Si, and then to β-tin Si. Upon further unloading, the β-tin Si can undertake several crystalline forms, changing to a metastable rhombohedral (R8, Si XII) solid structure at 8–10 GPa (Crain et al., 1994; Pfrommer et al., 1997; Piltz et al., 1995) and to a 1–2% denser body centered cubic silicon (bcc, Si III) at 2 GPa. Finally, at full unloading, amorphous Si appears (Tolbert et al., 1996).

The micro/nano-indentation tests have made further revelations of the complex phase changes in silicon (Callahan and Morris, 1992; Clarke et al., 1988; Domnich et al., 2000; Galanov et al., 1998; Gogotsi et al., 2000; Swain, 1998; Weppelmann et al., 1993; Williams et al., 1999; Zarudi and Zhang, 1999). It was found that the load–penetration curve in a loading/unloading cycle is hysteretic. Most interestingly, while the curve is smooth over a large interval, it suddenly jumps at some points, called pop-in/pop-out, regarded as the finite penetrations caused by a sudden volumetric reduction/expansion of a large volume of silicon during the transition from one phase to another. In their experiments on indentation with a spherical indenter, Zarudi and Zhang (1999) discovered that the denser ductile structure of the β-tin silicon in unloading undergoes a process from β-tin to bcc, and then to amorphous.

The findings of the experiments have been supported by theoretical studies in terms of the stability of the various silicon microstructures (Chang and Cohen, 1985; Cheong and Zhang, 2000a,Cheong and Zhang, 2000b; Duclos et al., 1990; Mizushima et al., 1994; Mylvaganam and Zhang, 2003; Piltz et al., 1995; Smith et al., 2000; Yin and Cohen, 1982; Zhang and Tanaka, 1999). At the atomic scale, Zhang and Tanaka (1999) did molecular dynamics (MD) simulations and found that the volume reduction at pop-in is about 20%. Cheong and Zhang (2000a) pointed out that the formation of the β-tin phase in loading is critical to the appearance of amorphous silicon after unloading.

The existing experimental and theoretical work has greatly contributed to the understanding of the microstructural changes, and consequently, the mechanical behaviour that silicon exhibits under external loads. However, a mechanical constitutive model capable of predicting the phase transitions of silicon does not exist. The formulations available, such as the von Mises and Drucker-Prager models, cannot produce consistent results with the experimental findings. In their finite element analysis of micro-indentation by a spherical indenter, Zhang and Mahdi (1996) have shown that the von Mises material formulation does not closely match the experimental load–penetration curve, and does not predict the observed pop-out.

This paper aims to develop a new constitutive model to accommodate the microstructural effect of phase transformations in silicon when subjected to complex loading conditions. Similar to the classical theory of plasticity, the model will introduce a series of threshold surfaces to mark the onset of plasticity and the subsequent phase transformations. After that, the plastic gradients are calculated from the plastic potential function, plastic flow and hardening rule.

2. Yield criterion

The constitutive laws used so far in predicting the behaviour of silicon through numerical simulations have been the conventional von Mises model and the Drucker-Prager model, Fig. 1; the former resting on the assumption that the yield surface is a right cylinder and that yielding does not depend on the hydrostatic stress. A model for pressure-sensitive materials is the Drucker-Prager model (Desai and Siriwardane, 1984) which recognizes the role of hydrostatic compression on yielding, but assumes that the conical yield surface

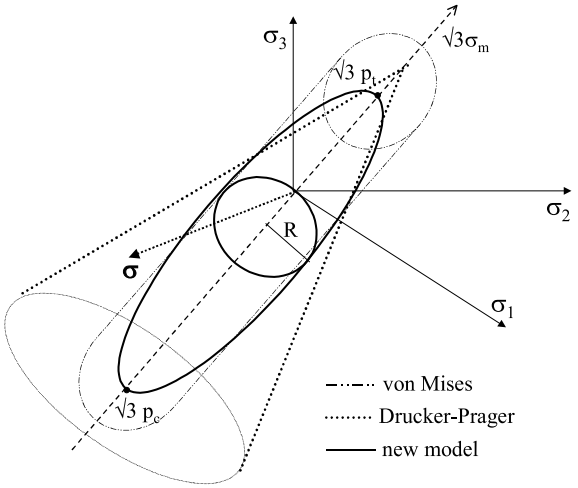

Fig. 1. Yield functions in principal stress space.

is open in the negative principal stress space. This is clearly not suitable for describing the mechanical behaviour of silicon, because, as discussed above, silicon has a series of definite phase transformation events in the negative principal stress space along its isocline. Hence, a more reliable prediction may be achieved if the yield surface for silicon is closed on both sides of the principal stress space.

Based on these considerations, five fixed (limiting) quadratic surfaces of closed ellipsoids are introduced, as shown in Fig. 2. The first surface is for the onset of plasticity, and the remaining ones are for the four subsequent phase transformation events in loading, from the initial diamond structure of silicon to its β-tin, ph, hcp, and fcc structures. When the stress level is low, the material is elastic and the stress point $\boldsymbol{\sigma}$ is inside the first limiting surface. The material becomes elastic–plastic when $\boldsymbol{\sigma}$ reaches the first yield surface. The deformation then develops according to a hardening law with the further increase of $\boldsymbol{\sigma}$. When $\boldsymbol{\sigma}$ reaches the first phase transformation surface, the material undergoes a sudden volumetric change and after that it hardens and moves further towards the following phase transformation surfaces. In unloading, phase changes have also been experimentally observed but at different hydrostatic thresholds. Therefore, another

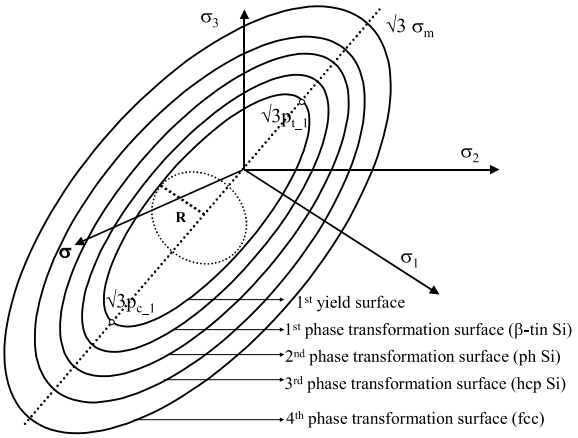

Fig. 2. Yield surface and phase transformation surfaces in loading, in principal stress space.

set of closed fixed phase transformation surfaces is defined, which pass through the experimental hydrostatic thresholds in unloading and are parallel to those in loading.

Let the second deviatoric stress invariant at time $t+\Delta t$ be ${}^{t+\Delta t}J_2$, the effective stress be ${}^{t+\Delta t}\overline{\sigma}^2 = 3{}^{t+\Delta t}J_2$, and the hydrostatic pressure be ${}^{t+\Delta t}\sigma_m$. The coordinates of a stress point in the three-dimensional principal stress space, along its isocline and in the perpendicular direction, are $\sqrt{3}{}^{t+\Delta t}\sigma_m$ and $\sqrt{2}{}^{t+\Delta t}J_2$, respectively. The yield surfaces are assumed to be continuous and ellipsoidal, centered at $\sqrt{3}\frac{{}^{t+\Delta t}p_t+{}^{t+\Delta t}p_c}{2}$ along the isocline of the space, thus

$$\frac{\left(\sqrt{3}{}^{t+\Delta t}\sigma_m - {}^{t+\Delta t}D\right)^2}{\left[\left(\sqrt{3}{}^{t+\Delta t}p_t - \sqrt{3}{}^{t+\Delta t}p_c\right)/2\right]^2} + \frac{\left(\sqrt{2^{t+\Delta t}J_2}\right)^2}{{}^{t+\Delta t}R^2} = 1, \tag{1}$$

where ${}^{t+\Delta t}p_t$, ${}^{t+\Delta t}p_c$ and ${}^{t+\Delta t}R$ are material constants (Fig. 2), and ${}^{t+\Delta t}D$ is the distance between the center of the ellipsoid and the origin of the coordinate system, i.e.,

$${}^{t+\Delta t}D = -\frac{\sqrt{3}({}^{t+\Delta t}p_t + {}^{t+\Delta t}p_c)}{2}. \tag{2}$$

Hence, the fixed and moving yield/phase transformation surface is defined in terms of the mean stress and the effective stress. If Eq. (1) is multiplied by $1.5{}^{t+\Delta t}R^2$, it gives rise to

$${}^{t+\Delta t}f({}^{t+\Delta t}\sigma_m, {}^{t+\Delta t}\overline{\sigma}^2, {}^{t+\Delta t}\varepsilon^{\mathrm{p}}_{ij}, {}^{t+\Delta t}p_t, {}^{t+\Delta t}p_c, {}^{t+\Delta t}R) = \frac{3}{2}\frac{{}^{t+\Delta t}R^2\left[{}^{t+\Delta t}\sigma_m - ({}^{t+\Delta t}p_t + {}^{t+\Delta t}p_c)/2\right]^2}{\left[({}^{t+\Delta t}p_t - {}^{t+\Delta t}p_c)/2\right]^2} + {}^{t+\Delta t}\overline{\sigma}^2 - \frac{3}{2}{}^{t+\Delta t}R^2 \equiv 0, \tag{3}$$

or simply,

$${}^{t+\Delta t}f \equiv 0, \tag{4}$$

which holds for all limiting and moving surfaces. In the case of a moving phase transformation surface, the state parameters vary with the external load and depend on the material properties and the hardening parameters.

3. Flow rule

The flow rule relates the plastic strain increments to the current stresses and stress increments. It is assumed that the normality rule and the associated flow law hold, i.e., the strain increments, $\Delta\varepsilon^{\mathrm{p}}_{ij}$, are normal to the plastic potential function and the plastic potential function is associated with the yield function. Thus, the plastic strain increments take the form

$$\Delta\varepsilon^{\mathrm{p}}_{ij} = \lambda\frac{\partial^{t+\Delta t}f({}^{t+\Delta t}\sigma_m, {}^{t+\Delta t}J_2)}{\partial^{t+\Delta t}\sigma_{ij}} = \lambda\frac{\partial^{t+\Delta t}f}{\partial^{t+\Delta t}\sigma_m}\frac{\partial^{t+\Delta t}\sigma_m}{\partial^{t+\Delta t}\sigma_{ij}} + \lambda\frac{\partial^{t+\Delta t}f}{\partial^{t+\Delta t}J_2}\frac{\partial^{t+\Delta t}J_2}{\partial^{t+\Delta t}\sigma_{ij}}, \tag{5}$$

where λ is the plastic multiplier, dependent on the hardening rule and the state variables at time t. Since

$$\frac{\partial^{t+\Delta t}\sigma_m}{\partial^{t+\Delta t}\sigma_{ij}} = \frac{1}{3}\delta_{ij}; \quad \frac{\partial^{t+\Delta t}J_2}{\partial^{t+\Delta t}\sigma_{ij}} = {}^{t+\Delta t}S_{ij}, \tag{6}$$

Eq. (5) reads

$$\Delta\varepsilon^{\mathrm{p}}_{ij} = \lambda\frac{{}^{t+\Delta t}R^2\left[{}^{t+\Delta t}\sigma_m - ({}^{t+\Delta t}p_t + {}^{t+\Delta t}p_c)/2\right]}{3\left[({}^{t+\Delta t}p_t - {}^{t+\Delta t}p_c)/2\right]^2}\delta_{ij} + \lambda{}^{t+\Delta t}S_{ij}. \tag{7}$$

In Eq. (7), the first term relates to the volumetric plastic strain increment,

$$\Delta\varepsilon_{\mathrm{v}}^{\mathrm{p}} = \lambda \frac{{}^{t+\Delta t}R^2\left[{}^{t+\Delta t}\sigma_m - ({}^{t+\Delta t}p_t + {}^{t+\Delta t}p_c)/2\right]}{\left[({}^{t+\Delta t}p_t - {}^{t+\Delta t}p_c)/2\right]^2}, \tag{8}$$

and the second term gives the plastic strain increments due to the deviatoric stresses. Eq. (7) shows that the vector of the inelastic strain increment is not in the direction of the deviatoric stress vector.

In loading, the plastic multiplier λ is positive. Eq. (8) indicates that the volumetric plastic strain $\Delta\varepsilon_{\mathrm{v}}^{\mathrm{p}} > 0$, if

$$\sigma_m - (p_t + p_c)/2 > 0. \tag{9}$$

Therefore, the volume of the material increases for mean stresses higher than the mean stress at the ellipsoid's center, and decreases when they are lower.

The plastic multiplier λ can be evaluated by taking a dot product of the increment of the plastic strain tensor in Eq. (7), which gives rise to

$$\lambda^2 = \frac{1}{3}\frac{\Delta\varepsilon_{ij}^{\mathrm{p}}\Delta\varepsilon_{ij}^{\mathrm{p}}}{2^{t+\Delta t}\overline{\sigma}^2 + \frac{{}^{t+\Delta t}R^4\left[{}^{t+\Delta t}\sigma_m - ({}^{t+\Delta t}p_t + {}^{t+\Delta t}p_c)/2\right]^2}{\left[({}^{t+\Delta t}p_t - {}^{t+\Delta t}p_c)/2\right]^4}}. \tag{10}$$

4. Post-yielding behaviour

The post-yielding behaviour is captured by the hardening law, which governs the modification of a yield surface during plastic flow. The rate of expansion/shrinkage of the surface is experimentally determined for simple stress states, and conclusions are then drawn for complex stress states. In this work, a pure hydrostatic pressure test is taken to define the hardening of silicon as the expansion of the yield surface perpendicular to the space diagonal is assumed to be given by $\Delta R = |\Delta p_c| = \Delta p_t$. Furthermore, it is assumed that the hardening is isotropic, i.e., the center of the yield surface does not move. It is worth emphasizing that although the moving surfaces should remain smooth and not intersect each other, their rate of expansion in the presence of deviatoric stresses may not be isotropic as assumed above. Nevertheless, this hypothesis can suffice as a first approximation and a refinement can be easily conducted when future experimental evidence becomes available.

5. Stress–strain relationship

The above yield function, flow rule, and hardening rule result in a relationship between the stress vector and strain vector. The stresses for a particular load depend not only on the material constants and total strains, but also on the plastic strains accumulated along the loading path. In the numerical procedure it is assumed that the stress/strain state is completely known at time t, and the total strains are assigned for time $t + \Delta t$. The current stresses at $t + \Delta t$ can be calculated as for an 'imaginary' elastic state obtained by unloading the material from the current stress state (Bathe, 1996). This is illustrated in Fig. 3, where $\boldsymbol{\sigma}$ and $\boldsymbol{\varepsilon}$ refer to the stress and strain states in general. The elastic strain components at $t + \Delta t$ are evaluated as the difference between the total strain components, ${}^{t+\Delta t}\boldsymbol{\varepsilon}^{\mathrm{T}}$, and the plastic strains, ${}^{t+\Delta t}\boldsymbol{\varepsilon}^{\mathrm{p}}$,

$${}^{t+\Delta t}\boldsymbol{\sigma} = \mathbf{C}^{\mathrm{e}\,t+\Delta t}\boldsymbol{\varepsilon}^{\mathrm{e}} = \mathbf{C}^{\mathrm{e}}\left({}^{t+\Delta t}\boldsymbol{\varepsilon}^{\mathrm{T}} - {}^{t+\Delta t}\boldsymbol{\varepsilon}^{\mathrm{p}}\right), \tag{11}$$

where $\mathbf{C}^{\mathrm{e}}$ is the elastic constitutive tensor. Furthermore, the plastic strains at $t + \Delta t$ are the sum of the plastic strains at t and the plastic strain increment from time t to $t + \Delta t$,

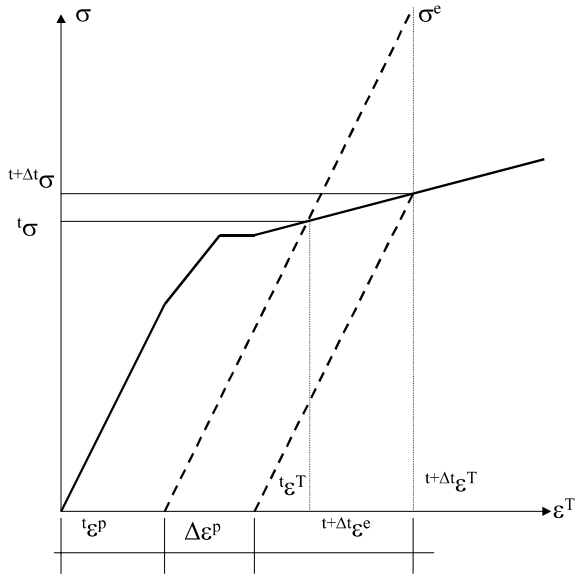

Fig. 3. Elastic–plastic material behaviour with a pop-in.

$$^{t+\Delta t}\boldsymbol{\varepsilon}^{\mathrm{p}} = {}^{t}\boldsymbol{\varepsilon}^{\mathrm{p}} + \Delta\boldsymbol{\varepsilon}^{\mathrm{p}}. \tag{12}$$

After expanding the right-hand side of Eq. (11), the formula for $^{t+\Delta t}\boldsymbol{\sigma}$ can be interpreted as the sum of an elastic predictor $^{t+\Delta t}\boldsymbol{\sigma}^{\mathrm{e}}$ for the response between t and $t+\Delta t$ ($\Delta\boldsymbol{\varepsilon}^{\mathrm{p}}$ is zero), and a stress correction that takes the stress vector back to its current state,

$$^{t+\Delta t}\boldsymbol{\sigma}^{\mathrm{cor}} = -C^{\mathrm{e}}\Delta\boldsymbol{\varepsilon}^{\mathrm{p}}. \tag{13}$$

Eqs. (13) and (7) show that the correction stress vector of the present model is not in the direction of the deviatoric stress vector, because it is altered by the mean stress.

By substituting Eq. (7) into Eq. (12), and then into Eq. (11), the general stress–strain relationship at $t+\Delta t$ can be written as a sum of the mean and the deviatoric stress components,

$$^{t+\Delta t}\sigma_{ij} = {}^{t+\Delta t}\sigma_m\delta_{ij} + {}^{t+\Delta t}S_{ij}, \tag{14}$$

where

$$^{t+\Delta t}S_{ij} = \frac{^{t+\Delta t}\varepsilon''_{ij}}{\frac{1+\mu}{E}+\lambda}, \tag{15}$$

$$^{t+\Delta t}\varepsilon''_{ij} = {}^{t+\Delta t}\varepsilon'_{ij} - {}^{t}\varepsilon^{\mathrm{p}}_{ij}, \tag{16}$$

$$^{t+\Delta t}\varepsilon'_{ij} = {}^{t+\Delta t}\varepsilon^{\mathrm{T}}_{ij} - {}^{t+\Delta t}\varepsilon^{\mathrm{T}}_{m}\delta_{ij}. \tag{17}$$

Clearly, Eq. (15) represents the first constitutive law (Bathe, 1996) and Eq. (17) gives the components of the deviatoric strain tensor.

The mean stress in Eq. (14) is

$$^{t+\Delta t}\sigma_m = 3K(^{t+\Delta t}\varepsilon''_m - \Delta\varepsilon^{\mathrm{p}}_m), \tag{18}$$

$$ {}^{t+\Delta t}\varepsilon''_m = {}^{t+\Delta t}\varepsilon^{\mathrm{T}}_m - {}^{t}\varepsilon^{\mathrm{p}}_m, \tag{19} $$

$$ {}^{t}\varepsilon^{\mathrm{p}}_m = \frac{{}^{t}\varepsilon^{\mathrm{p}}_{11} + {}^{t}\varepsilon^{\mathrm{p}}_{22} + {}^{t}\varepsilon^{\mathrm{p}}_{33}}{3} = \frac{{}^{t}\varepsilon^{\mathrm{p}}_{\mathrm{v}}}{3}, \tag{20} $$

which show the second constitutive law. In the above formulae ${}^{t+\Delta t}\varepsilon^{\mathrm{T}}_m$ is the total mean strain at $t+\Delta t$ and ${}^{t}\varepsilon^{\mathrm{p}}_m$ is the plastic mean strain at t.

In view of Eq. (8), for a complex stress state, Eq. (18) reads

$$ {}^{t+\Delta t}\sigma_m = \frac{3K^{t+\Delta t}\varepsilon''_m \frac{({}^{t+\Delta t}p_t - {}^{t+\Delta t}p_c)^2}{4} + K\lambda^{t+\Delta t}R^2 \frac{{}^{t+\Delta t}P_t + {}^{t+\Delta t}P_c}{2}}{\frac{({}^{t+\Delta t}p_t - {}^{t+\Delta t}p_c)^2}{4} + K\lambda^{t+\Delta t}R^2}. \tag{21} $$

By taking the dot product of the tensors in Eq. (15), the effective stress at $t+\Delta t$ becomes

$$ {}^{t+\Delta t}\overline{\sigma}^2 = \frac{{}^{t+\Delta t}d^2}{\left(\frac{1+\mu}{E} + \lambda\right)^2}, \tag{22} $$

where

$$ {}^{t+\Delta t}d^2 = \frac{3}{2}\,{}^{t+\Delta t}\boldsymbol{\varepsilon}''^{T} \cdot {}^{t+\Delta t}\boldsymbol{\varepsilon}''. \tag{23} $$

The formulae for the stress components at $t+\Delta t$ are therefore defined in terms of the assigned total strains, where the plastic multiplier λ is determined by the accumulated plastic strains along the loading path.

6. Tangent stress–strain matrix

Eq. (11) represents the integrated form of the incremental stress–strain relationship. In order to apply the finite element method for the stress integration, a tangent stress–strain matrix at $t+\Delta t$, which must be consistent with the numerical stress integration scheme, is required. To this end, let the stress and total strain states be defined in a vector form as

$$ {}^{t+\Delta t}\boldsymbol{\sigma} = \left\langle {}^{t+\Delta t}\sigma_1\ {}^{t+\Delta t}\sigma_2\ {}^{t+\Delta t}\sigma_3\ {}^{t+\Delta t}\sigma_4\ {}^{t+\Delta t}\sigma_5\ {}^{t+\Delta t}\sigma_6 \right\rangle, \tag{24} $$

$$ {}^{t+\Delta t}\boldsymbol{\varepsilon}^{\mathbf{T}} = \left\langle {}^{t+\Delta t}\varepsilon^{\mathrm{T}}_1\ {}^{t+\Delta t}\varepsilon^{\mathrm{T}}_2\ {}^{t+\Delta t}\varepsilon^{\mathrm{T}}_3\ {}^{t+\Delta t}\varepsilon^{\mathrm{T}}_4\ {}^{t+\Delta t}\varepsilon^{\mathrm{T}}_5\ {}^{t+\Delta t}\varepsilon^{\mathrm{T}}_6 \right\rangle, \tag{25} $$

$$ {}^{t+\Delta t}\varepsilon^{\mathrm{T}}_4 = {}^{t+\Delta t}\gamma_{12}, \quad {}^{t+\Delta t}\varepsilon^{\mathrm{T}}_5 = {}^{t+\Delta t}\gamma_{23}, \quad {}^{t+\Delta t}\varepsilon^{\mathrm{T}}_6 = {}^{t+\Delta t}\gamma_{31}, \quad {}^{t+\Delta t}\gamma_{ij} = {}^{t+\Delta t}\varepsilon^{\mathrm{T}}_{ij} + {}^{t+\Delta t}\varepsilon^{\mathrm{T}}_{ji}. \tag{26} $$

Then, the terms of the tangent elastic–plastic constitutive tensor can be calculated as the derivatives of the stress vector with respect to the total strain vector, i.e.,

$$ C^{\mathrm{ep}} = \frac{\partial^{t+\Delta t}\boldsymbol{\sigma}}{\partial^{t+\Delta t}\boldsymbol{\varepsilon}^{\mathrm{T}}}. \tag{27} $$

For a general loading, the derivatives of the normal stresses, ${}^{t+\Delta t}\sigma_i$ $(i=1,2,3)$, with respect to the corresponding total normal strains, ${}^{t+\Delta t}\varepsilon^{\mathrm{T}}_i$ $(i=1,2,3)$, become

$$ C^{\mathrm{ep}}_{ii} = \frac{\partial^{t+\Delta t}\sigma_m}{\partial^{t+\Delta t}\varepsilon^{\mathrm{T}}_i} + \frac{2}{3\left(\frac{1+\mu}{E} + \lambda\right)} - \frac{{}^{t+\Delta t}\varepsilon''_i}{\left(\frac{1+\mu}{E} + \lambda\right)^2} \frac{\partial\lambda}{\partial^{t+\Delta t}\varepsilon^{\mathrm{T}}_i}, \quad i = 1,2,3. \tag{28} $$

This matrix is symmetric with non-diagonal terms in the first three rows, i.e.,

$$C_{ij}^{\mathrm{ep}} = \frac{\partial^{t+\Delta t}\sigma_m}{\partial^{t+\Delta t}\varepsilon_j^{\mathrm{T}}} - \frac{1}{3\left(\frac{1+\mu}{E}+\lambda\right)} - \frac{{}^{t+\Delta t}\varepsilon_i''}{\left(\frac{1+\mu}{E}+\lambda\right)^2}\frac{\partial\lambda}{\partial^{t+\Delta t}\varepsilon_j^{\mathrm{T}}}, \quad i=1,2,3; \quad j=1,2,3; \quad i\neq j. \tag{29}$$

The derivatives of the normal stresses with respect to the shear strains can be calculated as

$$C_{ij}^{\mathrm{ep}} = \frac{1}{2}\frac{\partial^{t+\Delta t}\sigma_m}{\partial^{t+\Delta t}\varepsilon_{kl}^{\mathrm{T}}} - \frac{1}{2}\frac{{}^{t+\Delta t}\varepsilon_i''}{\left(\frac{1+\mu}{E}+\lambda\right)^2}\frac{\partial\lambda}{\partial^{t+\Delta t}\varepsilon_{kl}^{\mathrm{T}}} \quad \text{for } i=1,2,3;\ j=4,5,6;\ k=j-3;\ l=j-2 \text{ or } l=j-5 \text{ if } l>3. \tag{30}$$

The derivatives of the shear stresses with respect to the corresponding shear strains are given by

$$C_{ii}^{\mathrm{ep}} = \frac{1}{2\left(\frac{1+\mu}{E}+\lambda\right)} - \frac{{}^{t+\Delta t}\varepsilon_i''}{2\left(\frac{1+\mu}{E}+\lambda\right)^2}\frac{\partial\lambda}{\partial^{t+\Delta t}\varepsilon_i^{\mathrm{T}}} \quad \text{for } i=4,5,6, \tag{31}$$

$$C_{ij}^{\mathrm{ep}} = -\frac{{}^{t+\Delta t}\varepsilon_j''}{2\left(\frac{1+\mu}{E}+\lambda\right)^2}\frac{\partial\lambda}{\partial^{t+\Delta t}\varepsilon_j^{\mathrm{T}}} \quad \text{for } i=4,5,6; \quad j=1,2,3. \tag{32}$$

In taking the derivatives of the mean stress in Eq. (21), one needs to note that the plastic multiplier and the state parameters are variable. Thus, Eq. (10), in combination with the experimental material curve $\boldsymbol{\sigma}$–$\boldsymbol{\varepsilon}$, and the yield condition, Eq. (4), should also be differentiated.

7. Multi-linear material model

A complete definition of the material model requires quantitative evaluations of its material parameters, i.e. the elastic modulus E, Poisson's ratio μ, the dimensions of the fixed yield/phase transformation surfaces, the rate at which they move (hardening parameters), and a possible tensile cut-off. Traditionally, these material constants are provided by simple experiments, which induce uniform stress/strain conditions in the tested samples. Silicon, however, is a very different material whose phase changes are sensitive to the combination of hydrostatic and deviatoric stresses. Thus, the hydrostatic pressure test and indentation are suitable for the constitutive modelling of silicon.

For mono-crystalline silicon, MD simulations conducted by Mylvaganam and Zhang (2003) have suggested that a multi-linear approximation, as shown in Fig. 4, is reasonable. Thus, the formulae for the stress components and tangent stress–strain components derived above can be much simplified as follows.

The plastic multiplier in Eq. (10) in pure hydrostatic compression depends only on the mean stress at $t+\Delta t$. However, the mean stress also satisfies the yield criterion and it is the state variable ${}^{t+\Delta t}p_c$ as well. Thus, the plastic volumetric strain increment in Eq. (8) can be written as

$$\Delta\varepsilon_{\mathrm{v}}^{\mathrm{p}} = \frac{{}^{t+\Delta t}p_c - {}^{t}p_{c\_Y}}{K_{\mathrm{p}}}, \tag{33}$$

where ${}^{t}p_{c\_Y}$ is a state variable at time t and $K_{\mathrm{p}} = \frac{KK^{\mathrm{T}}}{K-K^{\mathrm{T}}}$ is the plastic bulk modulus. Now, the plastic multiplier in Eq. (10) takes a simpler form of

$$\lambda = -\frac{{}^{t+\Delta t}p_c - {}^{t}p_{c\_Y}}{K_{\mathrm{p}}}\frac{\frac{{}^{t+\Delta t}p_t - {}^{t+\Delta t}p_c}{2}}{{}^{t+\Delta t}R^2}. \tag{34}$$

The negative sign above leads to a positive plastic multiplier in loading and a negative one in unloading.

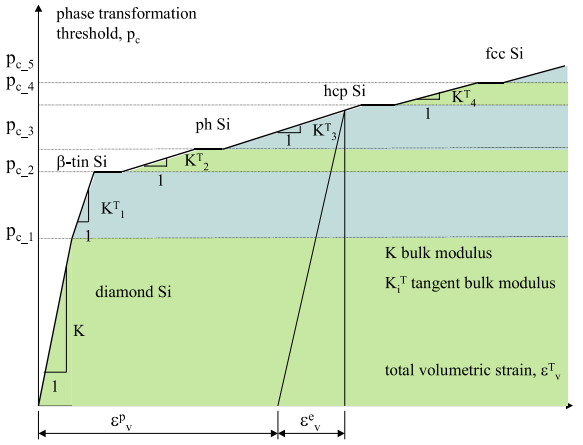

Fig. 4. Experimental working diagram of hydrostatic stress vs. volumetric total strain in pure hydrostatic compression.

Further, for a multi-linear hardening, Eq. (11) reduces to

$$ {}^{t+\Delta t}\sigma_m = \frac{3KK_{\mathrm{p}}\,{}^{t+\Delta t}\varepsilon''_m\,\frac{({}^{t+\Delta t}p_t - {}^{t+\Delta t}p_c)}{2} - K\frac{{}^{t+\Delta t}P_t + {}^{t+\Delta t}P_c}{2}\left({}^{t+\Delta t}p_c - {}^{t}p_{c\_Y}\right)}{K_{\mathrm{p}}\frac{({}^{t+\Delta t}p_t - {}^{t+\Delta t}p_c)}{2} - K\left({}^{t+\Delta t}p_c - {}^{t}p_{c\_Y}\right)}. \tag{35} $$

In taking the derivatives of the mean stress and the plastic multiplier, the yield criterion, flow rule and hardening rule need to be used. Letting $\Delta R = |\Delta p_c| = \Delta p_t$ Eqs. (34) and (35) become

$$ \frac{\partial\lambda}{\partial^{t+\Delta t}\varepsilon^{\mathrm{T}}_j} = \frac{\partial^{t+\Delta t}R}{\partial^{t+\Delta t}\varepsilon^{\mathrm{T}}_j}\,\frac{\frac{{}^{t+\Delta t}p_t - {}^{t+\Delta t}p_c}{2} - \left({}^{t+\Delta t}p_c - {}^{t}p_{c\_Y}\right) - 2K_{\mathrm{p}}\,{}^{t+\Delta t}R\lambda}{K_{\mathrm{p}}\,{}^{t+\Delta t}R^2}, \tag{36} $$

$$ \frac{\partial^{t+\Delta t}\sigma_m}{\partial^{t+\Delta t}\varepsilon^{\mathrm{T}}_j} = \frac{{}^{t+\Delta t}N_j}{K\left({}^{t+\Delta t}p_c - {}^{t}p_{c\_Y}\right) - K_{\mathrm{p}}\frac{{}^{t+\Delta t}p_t - {}^{t+\Delta t}p_c}{2}}, \tag{37} $$

where the numerator ${}^{t+\Delta t}N_j$ is calculated by

$$ {}^{t+\Delta t}N_j = -3KK_{\mathrm{p}}\frac{{}^{t+\Delta t}p_t - {}^{t+\Delta t}p_c}{2}\frac{1}{3} + \frac{\partial\Delta R}{\partial^{t+\Delta t}\varepsilon^{\mathrm{T}}_j}\left[-3KK_{\mathrm{p}}\,{}^{t+\Delta t}\varepsilon''_m + K\left({}^{t+\Delta t}\sigma_m - \frac{{}^{t+\Delta t}p_t + {}^{t+\Delta t}p_c}{2} + K_{\mathrm{p}}\,{}^{t+\Delta t}\sigma_m\right)\right] \quad \text{for } j = 1,2,3, \tag{38} $$

$$ {}^{t+\Delta t}N_j = \frac{\partial\Delta R}{\partial^{t+\Delta t}\varepsilon^{\mathrm{T}}_j}\left[-3KK_{\mathrm{p}}\,{}^{t+\Delta t}\varepsilon''_m + K\left({}^{t+\Delta t}\sigma_m - \frac{{}^{t+\Delta t}p_t + {}^{t+\Delta t}p_c}{2} + K_{\mathrm{p}}\,{}^{t+\Delta t}\sigma_m\right)\right] \quad \text{for } j = 4,5,6. \tag{39} $$

For the derivatives of R above, the yield criterion gives rise to

$$ \frac{\partial\Delta R}{\partial^{t+\Delta t}\varepsilon^{\mathrm{T}}_j} = \frac{-\frac{4}{3}\,{}^{t+\Delta t}\overline{\sigma}\,\frac{1}{\frac{1+\mu}{E}+\lambda}\,\frac{\partial d}{\partial^{t+\Delta t}\varepsilon_j} - 2KK_{\mathrm{p}}\,{}^{t+\Delta t}R^2\,\frac{\tau_n}{\tau_d^2}}{P} \quad \text{for } j = 1,2,3, \tag{40} $$

$$ \frac{\partial\Delta R}{\partial^{t+\Delta t}\varepsilon^{\mathrm{T}}_j} = \frac{-\frac{4}{3}\,{}^{t+\Delta t}\overline{\sigma}\,\frac{1}{\frac{1+\mu}{E}+\lambda}\,\frac{\partial d}{\partial^{t+\Delta t}\varepsilon_j}}{P} \quad \text{for } j = 4,5,6, \tag{41} $$

where

$$\tau_n = 3KK_{\mathrm{p}}{}^{t+\Delta t}\varepsilon''_m - K_{\mathrm{p}}\frac{{}^{t+\Delta t}p_c + {}^{t+\Delta t}p_t}{2}, \tag{42}$$

$$\tau_d = K_{\mathrm{p}}\frac{{}^{t+\Delta t}p_c - {}^{t+\Delta t}p_t}{2} - K({}^{t+\Delta t}p_c - {}^{t}p_{c\_Y}), \tag{43}$$

$$P = -\frac{4}{3}{}^{t+\Delta t}\overline{\sigma}^2\frac{\frac{{}^{t+\Delta t}p_t - {}^{t+\Delta t}p_c}{2} - ({}^{t+\Delta t}p_c - {}^{t}p_{c\_Y}) - 2K_{\mathrm{p}}{}^{t+\Delta t}R\lambda}{\left(\frac{1+\mu}{E} + \lambda\right)K_{\mathrm{p}}{}^{t+\Delta t}R^2} + 2^{t+\Delta t}R\left(\frac{\tau_n^2}{\tau_d^3} - 1\right) + 2^{t+\Delta t}R^2(K + K_{\mathrm{p}})\frac{\tau_n^2}{\tau_d^3} \tag{44}$$

8. Numerical applications

The constitutive model developed above can be applied to any type of loading. The integration of the stress–strain relationship can be implemented numerically. With the aid of ADINA, a commercially available FEA code, the formulae given in the previous sections are programmed in FORTRAN77 and supplied to the code as user-defined functions. The software assigns the total strains for each load increment, based on the provided elastic modulus. Then, it calls the user-supplied routines at each integration point for the calculation of the stresses, plastic strains and tangent stress–strain matrix. Some further details related to the implementation are listed in the Appendix A.

In order to validate the model two loading conditions are considered, a pure hydrostatic compression deducted from a MD simulation (Mylvaganam and Zhang, 2003) and an indentation carried out experimentally (Zarudi and Zhang, 1999).

8.1. Cubic silicon under hydrostatic compression

Under pure hydrostatic compression, Mylvaganam and Zhang (2003) revealed using MD simulations (Fig. 5) that the diagram of the mean stress vs. the total volumetric strain is almost linear initially until reaching a threshold of around 21 GPa, with a bulk modulus of 121.7 GPa. Then, within the zone $\sigma_m \in (21, 29)$ GPa, metallic silicon appears with an elastic–plastic behaviour, giving a tangent bulk modulus of 90.5 GPa. A second phase transformation, β-tin to hexagonal prism, is found in the range $\sigma_m \in (29, 33.5)$ GPa with a tangent bulk modulus of 54.1 GPa. To examine if the new constitutive model can predict the same results as MD, these material constants were applied to our FEA simulations as the hydrostatic pressure varied from zero to 33.5 GPa, Fig. 5. The sample was unloaded from 29 and 33.5 GPa, respectively. As unloading is linear elastic and the stress state is uniform, the unloading curve is a straight line. It is clear, as shown in Fig. 5, that the new model does reproduce the MD predictions. Fig. 5 also shows that the von Mises model can predict neither the plastic behaviour of silicon nor its phase transformation.

To demonstrate that the present model can accommodate sudden volumetric strains, causing the pop-ins/pop-outs phenomena, another FEA simulation is performed, Fig. 6. The pop-in is of 22% of the total volumetric strain, and it is assigned at the same threshold of 21 GPa as in Fig. 5. In unloading, to reflect the observation from MD simulations, it is assumed that the phase change happens in bulk silicon at a hydrostatic threshold of 16.2 GPa, with a volumetric expansion of 8% (Piltz et al., 1995).

If the von Mises material model is used in the FEA simulations, the stress–strain curve is a straight line in loading and unloading, as shown in Figs. 5 and 6. It is clear that the new material model is capable of characterising the plastic behaviour of pressure sensitive materials while the von Mises model is not.

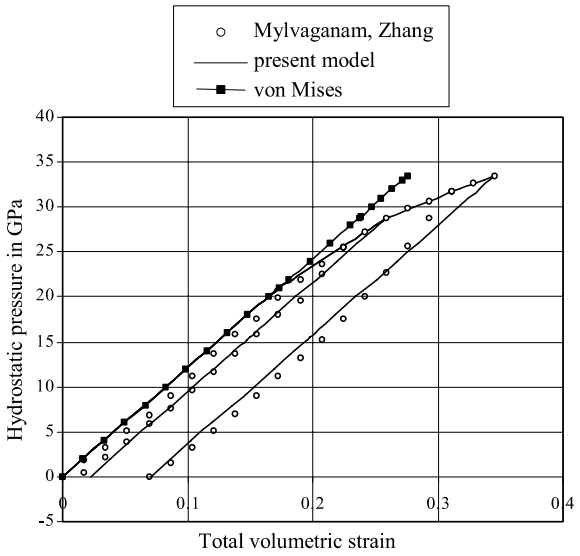

Fig. 5. Mean stress vs. total volumetric strain for elastic–plastic mono-crystalline silicon in hydrostatic stress state.

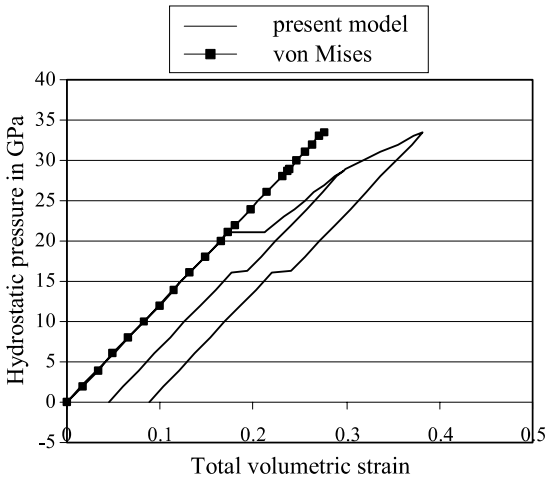

Fig. 6. Mean stress vs. total volumetric strain for elastic–plastic mono-crystalline silicon in hydrostatic stress state with a pop-in and a pop-out.

8.2. Nano-indentation

The present model was also applied to the indentation of silicon with a spherical indenter of 5 μm in radius and a maximum penetration of 320 nm (Vodenitcharova and Zhang, 2003). The relevant experiment was conducted by Zarudi and Zhang (1999). It is shown (Fig. 7) that the model predicts very well the experimental load–penetration curve. The material constants in the FEA simulations were derived by comparing the FEA results with the experimental data, and were found to be $E = 80$ GPa, $\mu = 0.17$; the hydrostatic thresholds in ascending order being 8.5, 10, 16, 40 and 79 GPa; the tangent bulk modulus being

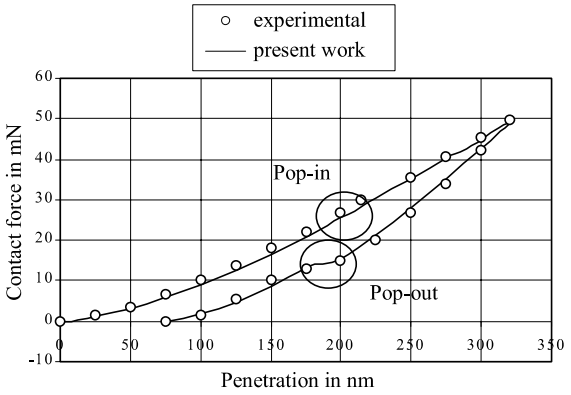

Fig. 7. Load–penetration curve of nano-indentation.

30 GPa for the diamond silicon, and 1 GPa for all subsequent solid phases. A volumetric reduction of 22% was assigned in loading at 10 GPa, which produced the observed pop-in in Fig. 7 at a penetration of around 210 nm. Upon unloading, at a penetration of around 200 nm, a well-defined finite displacement (pop-out) was recorded in the experiment. Applying the new constitutive model, the authors found that this sudden expansion could have been caused by a volumetric change in all the transformed material points of 80% of the total volumetric strain. More details on the FEA procedure and the variation of both the hydrostatic stress and the effective stress with the load and spatial coordinates can be found in another paper already published by the authors (Vodenitcharova and Zhang, 2003).

The values of E and μ are consistent with the literature reports, e.g. (Bever and Wert, 1990; www.design.caltech.edu/Research/MEMS/siliconprop.html; www.webelements.com/webelements/elements/text/Si/phys.html); the values of all other material parameters are consistent with the references mentioned in Section 1.

9. Conclusions

A new mechanical constitutive model has been developed for the multi-phase transformations of mono-crystal silicon, adopting the fundamental principles of the incremental theory of plasticity. The yield transformation surfaces used are closed and ellipsoidal. The model is capable of simulating complex behaviour of silicon such as pop-in and pop-out, which cannot be studied by any other existing continuum theories.

The current model can be extended to study other similar pressure-sensitive materials that have complicated solid phase transformations under mechanical loading.

Acknowledgements

The authors acknowledge the support of the following grants: ARC Large Grant, ARC IREX Award and The University of Sydney Sesqui Research Grant.

Appendix A

The steps of solution are similar to those given in the user-supplied options manual of ADINA, and outlined by Bathe (1996) for the von Mises model.

However, it needs to be noted that in contrast to the von Mises material, an exact solution for the stresses in the elastic–plastic zone at $t + \Delta t$ cannot be found from Eqs. (22) and (35) since the state variables are stress-dependent. A bisection scheme is therefore employed to solve Eq. (4) for ΔR, the distance between the current yield surface and the previous one. Then the state variables are updated,

$$^{t+\Delta t}R = {}^{t}R_Y + \Delta R, \quad {}^{t+\Delta t}p_c = {}^{t}p_{c\_Y} - \Delta R, \quad {}^{t+\Delta t}p_t = {}^{t}p_{t\_Y} - \Delta R. \tag{A.1}$$

The present model accounts for pops-in and pops-out. According to the experiments, the pops-in are sudden volumetric reductions at the point of phase transformation. In the present study, a finite inelastic strain, proportional to the total mean strain and the experimentally observed volumetric reduction, is added to the accumulated direct inelastic strains stored at time t:

$$^{t}\varepsilon_i^{\mathrm{p}} = \int_0^t \Delta\varepsilon_i^{\mathrm{p}} + p\frac{^{t}\varepsilon_{\mathrm{v}}^{\mathrm{T}}}{3}, \quad i = 1, 2, 3. \tag{A.2}$$

In the case of the phase change from diamond Si to β-tin, the pop-in, p, is taken as 22%. If the hydrostatic stress is compressive, the expression in Eq. (A.2) gives a volumetric reduction, and vice versa.

It is experimentally observed that the hydrostatic compressive thresholds in unloading are also accompanied by sudden volumetric changes. To account for this, a new set of limiting surfaces needs to be introduced, as mentioned in Section 2 of this paper. These surfaces are also ellipsoidal but are parallel to the corresponding loading surfaces at time t, and moving at a pace $\Delta R = |\Delta p_c| = \Delta p_t$. Again a bisection scheme is employed to update the state variables corresponding to the stress state at $t + \Delta t$.

If, however, the current 'phase transformation' surface in unloading is inside the elastic zone in loading, in further unloading it might fall entirely in the negative principal stress space. To avoid such unrealistic case, the state variables in the elastic zone in unloading are calculated proportional to the radius of the last yield surface, e.g. for the ith limiting surface,

$$^{t+\Delta t}R_i = p_{c\_i}\frac{^{t}R_Y}{^{t}p_{c\_Y}}, \tag{A.3}$$

$$^{t+\Delta t}p_{c/t} = {}^{t+\Delta t}R\frac{^{t}p_{c\_Y/t\_Y}}{^{t}R_Y}. \tag{A.4}$$

The pop-out in unloading is subtracted from the accumulated inelastic direct strains.

References

Bathe, J.K., 1996. Finite element procedures. Prentice Hall.

Bever, M.B., Wert, C.A., 1990. Mechanical Behaviour of Materials. McGraw-Hill Company.

Callahan, D.L., Morris, J.C., 1992. The extent of phase transformation in silicon hardness indentation. Journal of Materials Research 7, 1614–1617.

Chang, K.J., Cohen, M.L., 1985. Solid–solid phase transitions and soft photon modes in highly condensed Si. Physical Review B 31, 7819–7826.

Cheong, W.C., Zhang, L.C., 2000a. Effect of repeated nano-indentations on the deformation in monocrystalline silicon. Materials Science Letters 19, 439–442.

Cheong, W.C., Zhang, L.C., 2000b. Molecular dynamics simulations of phase transformations in silicon monocrystals due to nano-indentation. Nanotechnology 11, 1–7.

Clarke, D.R., Kroll, M.C., Kirchner, P.D., Cook, R.F., 1988. Amorphization and conductivity of silicon and germanium induced by indentation. Physical Review Letters 60, 2156–2159.

Crain, J., Ackland, G.J., Maclean, J.R., Piltz, R.O., Hatton, P.D., Pawley, G.S., 1994. Reversible pressure-induced structural transitions between metastable phases of silicon. Physical Review B 50, 13043–13047.

Desai, C.S., Siriwardane, H.J., 1984. Constitutive Laws for Engineering Materials, with Emphasis on Geologic Materials. Prentice-Hall.

Domnich, V., Gogotsi, Y., Dub, S., 2000. Effect of phase transformations on the shape of the unloading curve in the nanoindentaion of silicon. Applied Physics Letters 76, 2214–2216.

Duclos, S.J., Vohra, Y.K., Ruoff, A.L., 1990. Experimental study of the crystal stability and equation of state of Si to 248 GPa. Physical Review B 41, 12021–12028.

Galanov, B.A., Grigoriev, O.N., Gogotsi, Y.G., 1998. Effect of phase transformations on hardness of semiconductors. Materials Research Society Simposia Proceedings 481, 249–254.

Gogotsi, Y.G., Domnich, V., Dub, S.N., Kailer, A., Nickel, K.G., 2000. Cyclic nanoindentation and Raman microspectroscopy study of phase transformations in semiconductors. Journal of Materials Research 15, 871–879.

Hanfland, M., Schwarz, U., Syassen, K., Takemura, K., 1999. Crystal structure of the high-pressure phase silicon vi. Physical Review Letters 82, 1197–1200.

Hu, J.Z., Merkle, L.D., Menoni, C.S., Spain, I.L., 1986. Crystal data for high-pressure phases of silicon. Physical Review B 34,, 4679–4684.

McMahon, M.I., Nelmes, R.J., 1993. New high-pressure phase of Si. Physical Review B 47, 8337–8340.

McMahon, M.I., Nelmes, R.J., Wright, N.G., Allan, D.R., 1994. Pressure dependence of the *Imma* phase of silicon. Physical Review B 50, 739–743.

Mizushima, K., Yip, S., Kaxiras, E., 1994. Ideal crystal stability and pressure-induced phase transition in silicon. Physical Review B 50, 14952–14959.

Mylvaganam, K., Zhang, L.C., 2003. Atomic deformation of silicon under triaxial stresses. Key Engineering Materials 233–236, 615–620.

Pfrommer, B.G., Cote, M., Louie, S.G., Cohen, M.L., 1997. Ab initio study of silicon in the R8 phase. Physical Review B 56, 6662–6668.

Piltz, R.O., Maclean, J.R., Clark, S.J., Ackland, G.J., Hatton, P.D., Crain, J., 1995. Structure and properties of silicon XII: a complex tetrahedrally bonded phase. Physical Review B 52, 4072–4085.

Smith, G.S., Tadmor, E.B., Kaxiras, E., 2000. Multiscale simulation of loading and electrical resistance in silicon nanoindentation. Physical Review Letters 84, 1260–1263.

Swain, M.V., 1998. Mechanical property characterization of small volumes of brittle materials with spherical tipped indenters. Material Science in Engineering A 253, 160–166.

Tolbert, S.H., Herold, A.B., Brus, L.E., Alivisatos, A.P., 1996. Pressure-induced structural transformations in Si nanocrystals. Physical review Letters 76, 4384–4387.

Vodenitcharova, T., Zhang, L.C., 2003. A mechanics prediction of the behaviour of mono-crystalline silicon under nano-indentation. International Journal of Solids and Structures 40, 2989–2998.

Weppelmann, E.R., Field, J.S., Swain, M.V., 1993. Observations, analysis, and simulation of the hysteresis of silicon using ultra-micro-indentation with spherical indenters. Journal of Materials Research 8, 830–840.

Williams, J.S., Chen, Y., Wong-Leung, Kerr, A., 1999. Ultra-micro-indentation of silicon and compound semiconductors with spherical indenters. Journal of Materials Research 14, 2338–2343.

Wu, Y.Q., Yang, X.Y., Xu, Y.B., 1999. Cross-sectional electron microscopy observation on the amorphized indentation region in [0 0 1] single-crystal silicon. Acta Mater. 47, 2431–2436.

Yin, M.T., Cohen, M.L., 1982. Theory of static structural properties, crystal stability, and phase transformations: Application to Si and Ge. Physical Review B 26, 5668–5687.

Zarudi, I., Zhang, L.C., 1999. Structure changes in mono-crystal silicon subjected to indentation-experimental findings. Tribology International 32, 701–712.

Zhang, L.C., Mahdi, M., 1996. Plastic Behaviour of Silicon Subjected to Micro-Indentation. Journal of Materials Science 32 (21), 5671–5676.

Zhang, L.C., Tanaka, H., 1999. On the mechanics and physics in the nano-indentaion of silicon monocrystals. JSME International Journal Series A 31, 546–559.